ACS ES&T Air

Open Access

pubs.acs.org/estair

Article

Application of a Chemical Index to Aerosol Mass Spectrometry: Delta Plots and Functional Group Distributions

Rachel E. O'Brien,* Manjula Canagaratna, Xu He, Yeaseul Kim, Adam Nix, and Hannah S. Kenagy

Cite This: *ACS EST Air* 2026, 3, 1421−1434

Read Online

ACCESS | Metrics & More | Article Recommendations | Supporting Information

ABSTRACT: A better understanding of the chemical properties of organic aerosol (OA) particles will improve our ability to characterize their sources and predict their lifetime. The high-resolution time-of-flight aerosol mass spectrometer (HR-ToF-AMS) is widely used to measure OA in real time using thermal vaporization followed by electron ionization (EI). EI creates fragment ions that can be assigned to functional groups using delta analysis, a method of classifying mass spectra according to the presence of different chemically related ion series. In this study, we demonstrate the application of delta analysis to characterize molecular structures using a new visualization method. We also use delta analysis to quantify the functional group distribution with an average absolute error of ∼5−6% for individual standard molecules, comparable to the error observed for OA mixtures from biomass and coal combustion fit with Fourier transform infrared spectroscopy. Finally, we apply delta functional group analysis to AMS positive matrix factorization (PMF) factors across seven different field campaigns and find a similar composition across the more oxidized factors with about 55% acid and 26% alcohol groups. The analysis method described here can be applied to any HR-ToF-AMS data set to provide quantitative relative functional group distributions for OA mixtures.

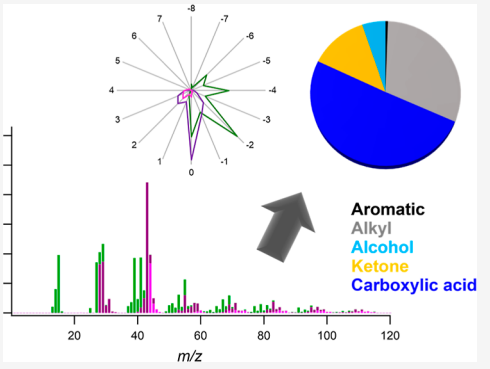

KEYWORDS: *functional groups, aerosol, aerosol mass spectrometer, delta analysis*

1. INTRODUCTION

Atmospheric organic aerosol (OA) particles are a large fraction of fine mode aerosol mass and they play important roles in climate and in human health.[1−3] Improving our understanding of their sources and lifetimes is essential for better predicting and managing their impacts. However, this is challenging because OA contains thousands of different organic compounds.[4,5] Many measurement methods used in the field provide only limited information on molecular structures for OA, but it is the chemical structures of the molecules in these organic mixtures that drive physical properties like viscosity, volatility, and hygroscopicity.[6−9] Thus, better methods to quantify molecular characteristics like functional groups will improve our ability to predict processes like particle growth or OA impact on cloud properties.

Numerous methods are used to characterize functional groups in OA samples. These methods include Fourier transform infrared spectroscopy (FTIR),[10−13] nuclear magnetic resonance spectroscopy (NMR),[14,15] soft ionization methods like electrospray ionization coupled with fragmentation,[16,17] and colorimetry.[18] While each of these methods has its strengths, all are designed for offline analysis and hence require collection of bulk samples. The aerosol mass spectrometer (AMS) is widely used in the field to measure OA in real time, and it provides quantitative information on total OA mass as well as elemental composition.[19,20] Multiple groups have combined AMS with FTIR analysis of collected filters to evaluate AMS fragment ions for interpretation of functional groups in the mixture.[13,21−23] These studies demonstrate the possibility for online AMS to provide information about functional groups, but they require direct comparisons with the OA filter samples.

Electron ionization, used in most AMS instruments, leads to extensive molecular fragmentation. EI spectra have been used for chemical identification with gas chromatography/mass spectrometry (GC/MS) since EI fragmentation patterns are related to the precursor's molecular structure.[24] However, AMS spectra of OA have fragments from thousands of chemicals, so individual chemical identification is usually not carried out. In addition, the range of chemicals measured with the AMS is broader than what is typically measured with GC/MS, which is generally limited to chemicals that are volatile at temperatures up to ∼300 °C, or slightly higher with derivatization.[25] In contrast, the AMS measures everything in OA that can volatilize off a heater at 600 °C. Changes occur to

Received: February 14, 2026
Revised: April 23, 2026
Accepted: April 24, 2026
Published: April 29, 2026

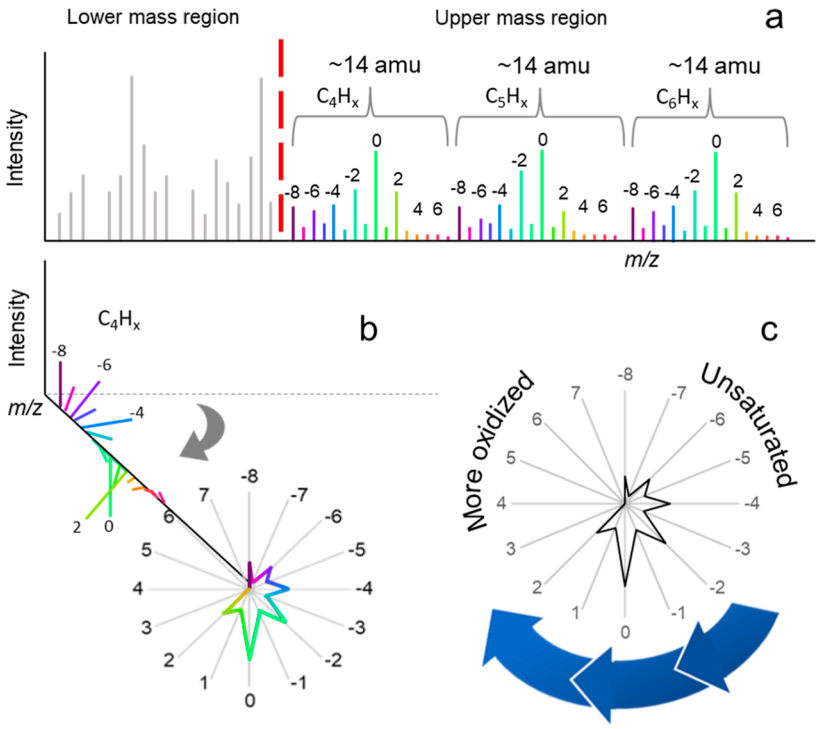

Figure 1. Figurative mass spectrum and delta plots showing the relationships between the delta values, carbon numbers, and the radial delta plots. (a) Figurative mass spectrum with delta values labeled above the ions (only even delta values are listed, for clarity) with both the lower (gray, below 48 m/z) and the higher mass regions (colors, above 48 m/z). (b) a portion of the spectrum viewed looking down the x-axis with a sequential rotation at each mass unit. (c) General trends in terms of the types of fragments across the delta values.

the chemicals during this thermal vaporization or pyrolysis, including the fragmentation and volatilization of functional groups. For example, acids can decarboxylate (lose CO_2) or dehydrate (lose H_2O) and alcohols dehydrate or experience dehydrogenation (loss of H_2 to form an aldehyde).[26] When dehydration occurs, the original molecule gains one degree of unsaturation for each water lost. Alkanes fragment on C−C bonds producing radicals and these can undergo radical propagation reactions that can add one or more degrees of unsaturation.[26] The combination of pyrolysis and fragmentation from EI generates more lower mass ions in AMS spectra compared to what is typically observed for GC/MS.[27,28]

The similarities between GC/MS and AMS data suggest that we can use methods developed for GC/MS, but that modifications are needed to account for more extensive fragmentation and more oxidized precursors. The delta analysis was developed in the 1970s as a classification system for EI spectra to help optimize GC/MS library searches.[29] This analysis groups ion fragments that differ only in the number of methylene, or CH_2, units. These homologous series are a subset of fragment ions observed for molecules in EI, and they can provide information on the identity of an unknown. The most familiar of these is the alkane fragment ion series at 43, 57, 71, 85 m/z, etc. Each series reflects carbon skeletons with different functional groups, so the amount and types of these homologous series in the spectrum can be directly related to the molecular structures and the functional groups present in the OA mixture.[24]

Since AMS mass spectra of OA contain thousands of different molecules and are thus too complicated to be characterized by a library fingerprint analysis, a classification tool like delta analysis is useful. Several prior studies have applied delta analysis to AMS spectra to look at trends in OA aging and differences in composition.[30−32] In this work, we build on this type of analysis by introducing the use of radial delta plots to map the fragment ions in an AMS spectrum, turning a complicated linear spectrum into shapes that are much easier to compare and discuss. The functional group quantification methods described here use the delta series identification rules built by McLafferty & Turecek (1993) for GC/MS with adjustments to account for the additional thermal decomposition and fragmentation that occurs in the AMS.

Overall, we find that radial delta plots of polyfunctional organic standards have distinct patterns related to their structures. With this framework, we quantify the relative fractions of carboxylic acids, alcohols, carbonyls, aromatics, and alkyl functional groups from individual AMS mass spectra. We demonstrate the application of this delta analysis to AMS data sets for standards and published spectra, and we provide reference tables to aid in interpretation. The work here is an introduction to radial delta plots that are generated from AMS spectra, and it provides a framework that can be used to calculate quantitative functional group distributions directly from any HR-ToF-AMS mass spectrum.

2. MATERIALS AND METHODS

Data sets used in this manuscript were obtained from the High Resolution AMS Spectral Database[33,34] as well as mass spectra used to calibrate elemental ratios for the AMS[35] and AMS spectra from a study comparing FTIR and AMS data sets.[23] Chemical structures were generated with ChemDraw (version 25.0.2.14) and mass spectra were visualized and created for the Table of Contents art using MARMOT v3.5A.[36] For delta plots used for qualitative analyses, all peaks below 48 m/z were removed to avoid the signal being dominated by large intensity, low mass ions that are commonly observed in AMS spectra, and the mass spectrum was renormalized.

https://doi.org/10.1021/acsestair.6c00059
ACS EST Air 2026, 3, 1421−1434

For the analysis of functional group distributions, the full mass spectrum was used. Isotopes were removed for these calculations because they are not always included in published peak lists. We did not include ions with nitrogen, sulfur, phosphorus, or chlorine as they were low in abundance for the data sets shown here.

2.1. Radial Delta Plots

An index was developed in the 1970s termed the Delta analysis, and it has the formula

$$\Delta = M - (14^{*}n) + 1 \tag{1}$$

where M is the mass of the ion and n is the total number of carbon, oxygen, or nitrogen atoms in that ion.[24,29] This equation groups ions based on "equivalent CH_2 units," i.e. separated in mass by multiples of 14 m/z. Ions that lack hydrogen (more unsaturated/aromatic) are found at the most negative delta values, and the delta values increase with increasing levels of saturation. Alkanes produce ions with a delta value of +2Δ. When oxygen is present, each oxygen atom adds +2 to the delta value because oxygen is 16 amu and is being compared as an equivalent $-CH_2$ unit (14 amu).

Figure 1 shows how radial delta plots of AMS mass spectra are constructed. In Figure 1a, the repeating cycle of the delta values for CH containing ions can be seen with each ∼14 amu section having the same number of carbons and different numbers of hydrogen atoms across the group. For a delta plot, if you shift the orientation of the mass spectrum to look down along the x-axis, the spectrum can be sequentially rotated so that each mass with the same color points in the same direction (Figure 1b). This groups the data so that all the ions with the same delta value point in the same radial direction, here labeled from −8Δ to +7Δ.

Figure 1c shows an example radial delta plot for CH containing ions from an OA sample with signal observed at delta values from −8Δ to +2Δ. The distance from the origin represents the total summed intensities for all the ions at that delta value. Since this is a histogram, the delta values are discrete values, but we plot them with connecting lines to improve the visual comparison, especially when multiple delta plots are overlaid. In addition, as will be discussed below, a very useful comparison is the relative intensities between odd vs even delta values. Thus, the lines connecting the delta values also help show relative differences. Overall, these radial histograms help visualize the contributions of different fragment types in the samples.

2.2. Functional Group Calculations

To obtain the weight fractions of the different functional groups, the mass for each functional group (M_{funct}) is first calculated from the relative intensities of ions that correspond to the individual functional groups using eq 2

$$M_{funct} = \sum_j \frac{MW_{funct}}{MW_j} \times I_j \tag{2}$$

where MW_{funct} is the molar mass of the functional group (Table S1), MW_j is the molar mass of the jth ion that is attributed to that functional group, and I_j is the relative intensity of that ion. Here, we assume that all functional groups can be present in each mass spectrum. After summing the ions identified for each functional group, the total mass across all functional groups is normalized to calculate the relative mass fraction (F_{funct}) of each functional group in the sample. These functional groups include alkyl, aromatics, carboxylic acids, alcohols, and ketones. There are a few ions that have fractional assignments between two different functional groups and these assignments are described in more detail below in Section 3.2.

The measured fractions of functional groups are expected to be different compared to the actual fractions due to loss of neutrals, including loss of H_2O from acids and alcohol groups. To correct for this, the O/C measured using the Improved Ambient method (IA)[35] is used to constrain the relative fraction of alkyl/aromatic vs carboxylic acids and alcohol groups. The O/C for the calculated functional group distribution is determined by calculating the relative number of oxygen (N_o) and carbon (N_c) atoms

$$N_O = \sum_i \frac{MW_{O,i}^{tot}}{MW_{funct,i}} \times \frac{F_{funct,i}}{MW_O} \tag{3}$$

$$N_C = \sum_i \frac{MW_{C,i}^{tot}}{MW_{funct,i}} \times \frac{F_{funct,i}}{MW_C} \tag{4}$$

where MW_O^{tot} and MW_C^{tot} are the total molar masses of the carbon and oxygen atoms in each functional group, F_{funct} is the relative mass fraction of each functional group in the spectrum, MW_{funct} is the molar mass of the functional group (Table S1), and MW_O and MW_C are the molar mass of oxygen and carbon, respectively. The i indicates that the equations are applied to each functional group and the total is summed and the values from eqs 3 and 4 are divided to give the O/C estimate.

If the O/C calculated from the F_{funct} values is lower than the measured IA O/C, then oxygen signal from alcohols and acids is considered to have been lost via dehydration. Typically, thermal decomposition results in the loss of CO, CO_2, and H_2O from oxidized species. The CO^+ and CO_2^+ ions can be represented in delta groups, but the H_2O^+ ion is not, so it needs to be accounted for by empirically adjusting the value of x in the equations below such that the calculated O/C from functional groups using eqs 3 and 4 matches that from the IA method. For this adjustment, the fraction of the signal that is removed from the alkyl/aromatic signal is split between the alcohol and the carboxylic acid fractions according to their ratio in the initial calculated fractions. This weighting can be changed in the future if it is determined that water is lost preferentially by functional group. The equations for the corrected weight fractions (CF) are provided below

$$CF_{alkyl} = F_{alkyl} - x_1\left(\frac{F_{alkyl}}{F_{alkyl} + F_{aromatic}}\right) \tag{5}$$

$$CF_{aromatic} = F_{aromatic} - x_1\left(\frac{F_{aromatic}}{F_{aromatic} + F_{alkyl}}\right) \tag{6}$$

$$CF_{acid} = F_{acid} + x_1\left(\frac{F_{acid}}{F_{acid} + F_{alcohol}}\right) \tag{7}$$

$$CF_{alcohol} = F_{alcohol} + x_1\left(\frac{F_{alcohol}}{F_{acid} + F_{alcohol}}\right) \tag{8}$$

here F_{alkyl} is the weight fraction of the alkyl functional group defined above (F_{funct}) and similarly for aromatics, alcohols, and carboxylic acids. The weight fraction of the oxygen (carbon) atoms is calculated by multiplying the corresponding equations above by the fraction of functional group mass attributable to oxygen (carbon) atoms. These weighted correction equations are summed for each atom (carbon and oxygen), the ratio of these totals is set equal to the O/C calculated with the improved ambient method, and the equation is solved for x_1. For this calculation, the O/C is adjusted to the weight fraction (i.e., multiplication of the O/C by 16/12) to match the weight fraction equations above (eqs 3 and 4). With x_1 determined, the new values of the corrected weight fractions of the functional groups are obtained.

If the O/C value is found to be greater than the O/C from the IA method, then a similar correction method is applied, but now the ketone fraction is included so that equal relative fractions of the signal from the acids, alcohols, and ketones are moved to the alkyl and aromatic fractions. These equations are shown in supplemental Section S1 and they are similar to eqs 5−8 with the addition of the ketone. Conceptually, the first correction is fixing an observed oxidized fragment signal that is too low due to loss of water during thermal desorption and ionization. This should only apply to alcohols and carboxylic acids, so only these two are included. The second type of correction is fixing an observed oxidized fragment signal that is too high, possibly due to thermal decomposition resulting in a small loss

https://doi.org/10.1021/acsestair.6c00059
ACS EST Air 2026, 3, 1421−1434

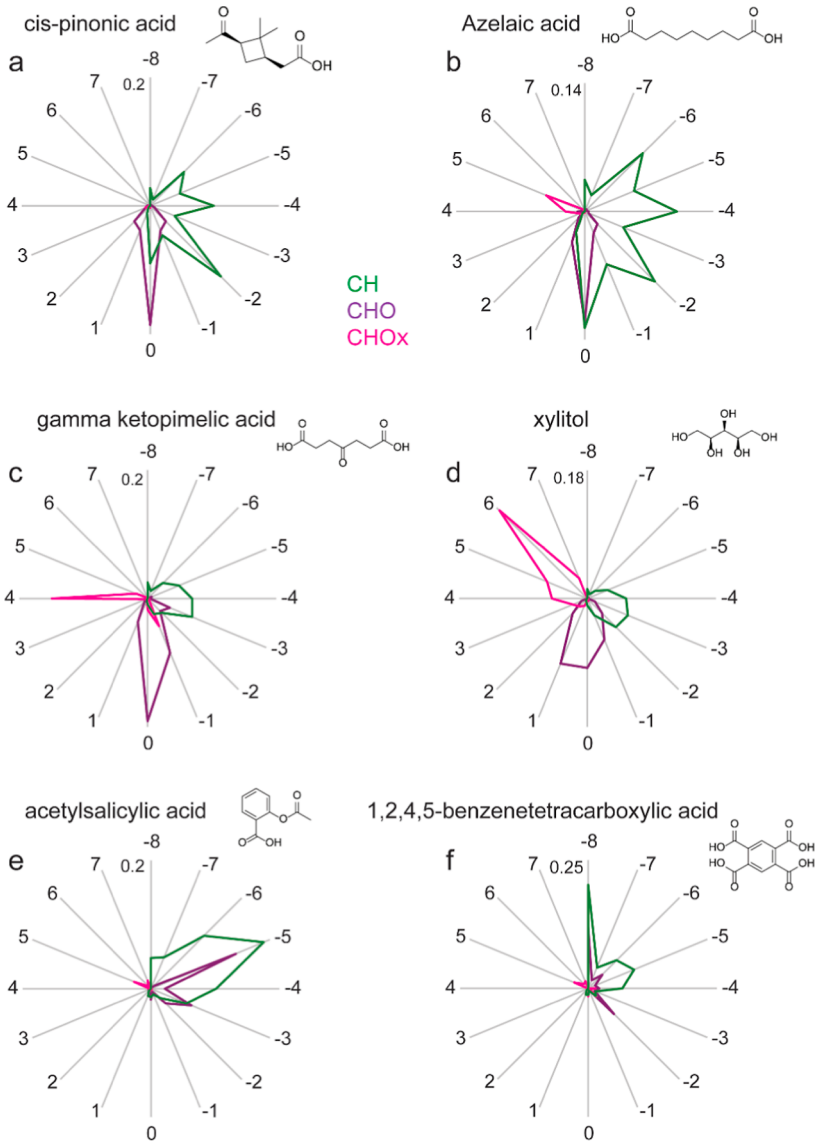

Figure 2. Delta plots for select standard chemicals: *cis*-pinonic acid, azelaic acid, gamma ketopimelic acid, xylitol, acetylsalicylic acid, and 1,2,4,5-benzenetetracarboxylic acid. The name and structure of the chemical is provided above each plot. The three different classes are overlaid with CH in green, CHO_1 in purple, and CHO_x in pink. The spectra are all normalized to a sum of one, and the maximum intensity is given at the top, offset from the top radial line.

of carbon signal. For this, all three types of oxidized fragments are included in the correction.

For the standards here, we use the O/C from the chemical structure for the corrections in order to avoid adding uncertainty from the measured O/C values for the individual compounds.[35] For the OA data sets, we use the O/C measured from the AMS spectrum. For all analyses, we report the average of the absolute value of the difference between the predicted fractions and the expected fractions based on the structure for the standards, or the fractions reported in the literature for the OA comparisons.

3. RESULTS AND DISCUSSION

3.1. Delta Pots of Chemical Standards

3.1.1. CH Traces. Here we present example delta plots from standards that contain different oxidized functional groups.[35] Delta plots for additional standards are collected in the supplemental (Section S2). Starting with the CH components (green), the overall intensity of the even delta values is higher than the odd values for both *cis*-pinonic and azelaic acid (Figure 2a,b), producing a distinct star shaped pattern. For C, H, and O containing ions, even delta values correspond to even electron ions. In EI, a radical cation ($M^{+\cdot}$) is initially generated that contains an odd number of electrons. Fragmentation of a single bond leads to the formation of an even electron ion and a neutral radical.[24] Thus, the higher abundance of even delta values in Figure 2a and b is characteristic of this type of fragmentation being the dominant ionization pathway for these ions.

The star pattern extends to negative delta values indicating that higher degrees of unsaturation in ion fragments are observed in the AMS even for molecules like azelaic acid that have no carbon−carbon double bonds in the original structure. The formation of unsaturated ions during fragmentation through the loss of H_2 and CH_4 is also observed to a smaller degree in GC/MS EI data and because of this, the CH ions with the highest delta value (i.e., the most hydrogen atoms) are recommended for use in identifying unknown molecules.[24] The presence of functional groups also affects CH

https://doi.org/10.1021/acsestair.6c00059
ACS EST Air 2026, 3, 1421−1434

fragmentation patterns. For example, azelaic acid contains a fully saturated alkyl section and one might expect to see intensity only at +2Δ like hexadecane (Figure S1a) if it lost both carboxylic acids to thermal decomposition during vaporization and the alkyl portion remained unchanged (e.g., no pyrolysis reactions leading to the formation of unsaturated fragments). However, there is instead minimal signal at +2Δ for CH fragments from chemicals containing an alkyl portion with two oxidized groups attached like azelaic acid.

The other four delta plots in Figure 2 show very different shapes compared to the star-like pattern. For example, ketopimelic acid and xylitol both show a more oblong shape with similar intensity on the odd and even delta values (Figure 2c,d). Odd delta values correspond to odd electron ions, which are formed when two bonds are broken off the charged species during fragmentation. This is observed for rings that break into two pieces, for dehydration, or for ions that undergo rearrangements prior to fragmentation. For example, a McLafferty rearrangement involves a shift in hydrogen and then fragmentation, resulting in two broken bonds between the products (ion and neutral).[24] A McLafferty rearrangement is likely for azelaic acid and the product for that will be discussed below for CHO_x ions. For CH ions, higher signal at odd delta values suggests a structure contains a relatively high amount of oxidized groups that can dehydrate during fragmentation, or rings that can fragment. Looking at the structures of ketopimelic acid and xylitol, the oxygen atoms are dispersed across the carbon backbone. Thus, for oxidized chemicals, greater intensity on the odd mass ions and an oblong (as opposed to star) shape can correspond to chemical structures with more functional groups interspersed throughout rather than isolated on the ends of the structures.

The spectra for 1,2,4,5-benzenetetracarboxylic acid and acetylsalicylic acid, two oxidized aromatics, have CH ions with more intensity at negative delta values (Figure 2e,f). This is consistent with the trend that more negative delta values correspond to more unsaturated ion fragments. Their shapes are not the same, with much more intensity at −8Δ for 1,2,4,5-benzenetetracarboxylic acid compared to acetylsalicylic acid. A full characterization of the behavior of oxidized aromatics will require future analysis of additional poly functional aromatic standards. It is likely that the ester directly attached to the aromatic ring on acetylsalicylic acid leads to different fragmentation pathways compared to the four carboxylic acids on benzene-tetracarboxylic acid. For the standards we have analyzed, minimal signal is observed at −8Δ unless an aromatic ring is present.

3.1.2. CHO_1 and CHO_x Traces. These standards also show CHO_1 (purple) and CHO_x (pink) containing ions (Figure 2). Lower signals for the CHO_x ions are observed for *cis*-pinonic, acetylsalicylic, and 1,2,4,5-benzenetetracarboxylic acid (pink traces, 2a, e, f). Carboxylic acids can decarboxylate during thermal vaporization to generate signal at CO_2^+, H_2O^+, and CO^+ and these delta plots only include ions greater than 48 *m/z*, so it it not surprising that less signal is seen for CHO_x ions. Other standard molecules that contain carboxylic acids show some CHO_x ions, so small CHO_x signal above 48 *m/z* is not a universal feature for carboxylic acid containing molecules. As an example, the clear CHO_x signal for azelaic acid at +5Δ is mostly due to $C_2H_4O_2^+$ which comes from a McLafferty rearrangement of a carboxylic acid.[24] For CHO_1 ions (purple), the most common intensity is 0Δ and the dominant ion at 0Δ*is* $C_3H_3O^+$ (Figure 2a, b, and c). Given the strong signal for this ion for chemicals containing acid groups (Figure 2), higher intensity at this ion suggests the presence of carboxylic acids.

All of the standards here and in supplemental Section S2 show delta plots that are characteristic of their structures. For these standards, we find that chemicals with longer alkyl segments show a star-like pattern with varying sharpness of the peaks due to variability in the amount of odd electron ions formed. Sharpness refers to the relative intensity differences between the even vs odd delta values. Shorter alkyl segments still give star patterns, but these appear narrower in width and generally less sharp. Chemicals that contain rings or many alcohol groups show oblong shapes. Aromatic chemicals have signals at −8Δ and some oblong characteristics. For OA, it is important to remember that the delta plots will be combinations of the spectra for all chemicals in the samples. Thus, a sample could have a 'less distinct' star pattern because some chemicals are highly oxidized while other components of the mixture contain longer alkyl segments. A summary of recommendations for interpreting delta plots is provided in Section S3. In the next section, we will apply the delta analysis framework to quantify functional groups.

3.2. Delta Plots and Functional Groups

The radial delta plots discussed above can help visualize where ions with different functional groups are expected. As noted, only the higher mass ions are used to minimize the impact of large intensity lower mass ions in AMS mass spectra. However, for the functional group quantification, the full mass spectrum is used. Tables of delta series and their corresponding functional groups are available for GC/MS analysis in McLafferty & Turecek, 1993.[24] For AMS data, we can use the same delta tables developed for GC/MS with some modifications due to the extra heat from the thermal desorption leading to extra fragmentation. Figure 3 shows illustrative delta plots labeled with the dominant functional group at each delta value. The colored regions are added to help guide the eye; the distance out from the center does not correlate with observations of intensities. For CHO_1 ions (purple, Figure 3a), the alcohol fragments tend to be found at +5Δ to +3Δ, the ketone fragments at +2Δ, and the acids between +1Δ and −2Δ with the largest intensity usually at 0Δ. The acid fragments for CHO_1 ions are forming through dehydration. For all these ions, the starting compound is assumed to be fully saturated. There will be some overlap on the odd electron ions between the functional groups, but they are usually lower intensity. They have been assigned following the more prevalent functional groups observed in the standards here.

In Figure 3b, the CHO_2 ions (pink) are shown with the largest signal for acids/esters at +4Δ and, for ions that have undergone McLafferty rearrangements, also at +5Δ. Figure S6 shows the oxidized fragments for azelaic acid with the largest +5Δ ion $C_2H_4O_2^+$ at 60 *m/z* and the largest +4 ion $C_3H_5O_2^+$ at 73 *m/z*, both of which are also characteristic ions for levoglucosan.[37] Apportioning intensity from these two ions between acids and levoglucosan is applied using rules based on the relative intensity of $C_2H_4O_2^+$. The largest relative intensity for $C_2H_4O_2^+$ (f_{60}) observed for these standards is 2.3%, so both 60 and 73 *m/z* are pooled into acids when f_{60} is below 2.5%. This is about a factor of 10 more than the background f_{60} of 0.3%, which is typically observed in ambient environments with mixed aerosol sources that do not contain biomass burning.[38] For values of f_{60} greater than 2.5%, this ion likely has

https://doi.org/10.1021/acsestair.6c00059
ACS EST Air 2026, 3, 1421−1434

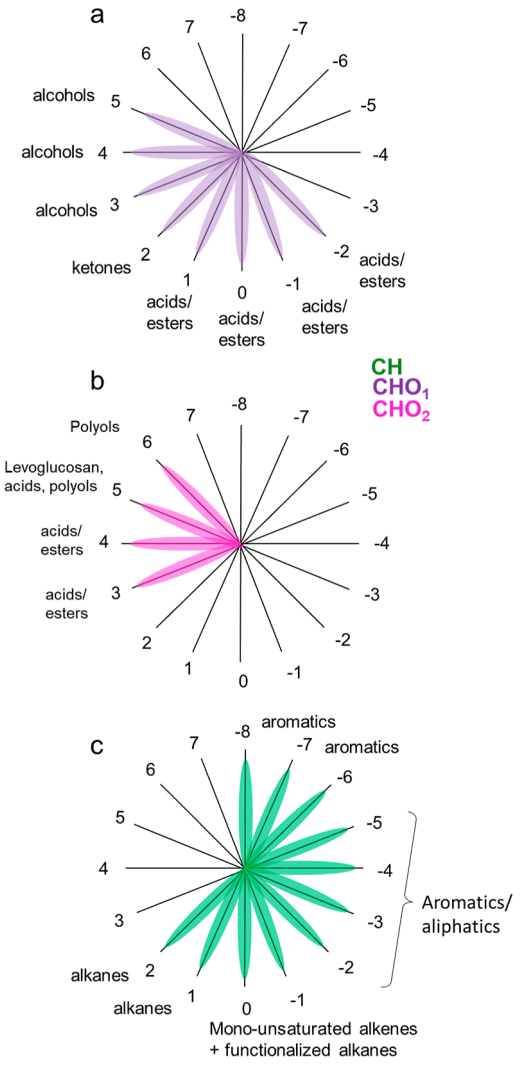

Figure 3. Figurative delta plots showing where fragments corresponding to different functional groups are expected.

a larger contribution from levoglucosan and can be pooled into alcohols. The above thresholds are based on aliphatic acids, which can undergo McLafferty rearrangements. More standards are needed for oxidized aromatics, but for biomass burning OA with mostly aromatic acids, the threshold will likely be a little lower.

The delta plot for the CH-containing ions is shown in Figure 3c (green). The typical range observed for these ions spans +2Δ to −8Δ with fully saturated alkanes at +2Δ and +1Δ, alkenes and functionalized alkanes at 0Δ and −1Δ, and aromatics at −7Δ and −8Δ. Ions with more negative delta values than −8Δ are all grouped at −8Δ and high intensity on these ions is only observed for standards that contain aromatic rings (Figures 2, S1−S5). Ions with delta values between −2Δ and −6Δ are observed to form from both aliphatic and aromatic chemicals. To separate these, we set a preliminary threshold for the fraction of CH signal at −8Δ to a value of 3%. When the signal for −8Δ is greater than this, all the intensity for CH ions with a hydrogen to carbon ratio (H/C) less than or equal to 1 is included in the aromatic pool. If the fraction is less than this, all the intensity for negative delta values more positive than −7Δ is included in alkyl. This gives an improved lower bound for the aromatic signal. Future studies with a wider range of aromatic chemicals can provide a better constraint on this weighting and thresholding.

The ion series listed above and shown in Figure 3 can generally be used to identify the functional group for a given fragment ion. However, there are three main exceptions. First, there are characteristic ions like CO_2^+ formed through decarboxylation of acids on the heater.[35] Second, alcohols show a high intensity ion at CHO_1^+ (29 m/z, + 2Δ) and polyols show ion intensity spanning down to −2Δ. This range for polyols has some overlap with the acids, so ions in this range are selected carefully based on these standards. Third, there are some overlaps for ions such as $C_2H_3O^+$ between acids, ketones, and alcohols. We note that these overlaps are similar to the uncertainty from overlapping FTIR signals across the OH stretching region and in the carbonyl region.[10] Examples and a discussion of dehydration of alcohols and acids is provided in the supplement (Section S4). Tables summarizing all the fragment ions, formulas, delta values, and sources are also provided (Section S5). Finally, a summary

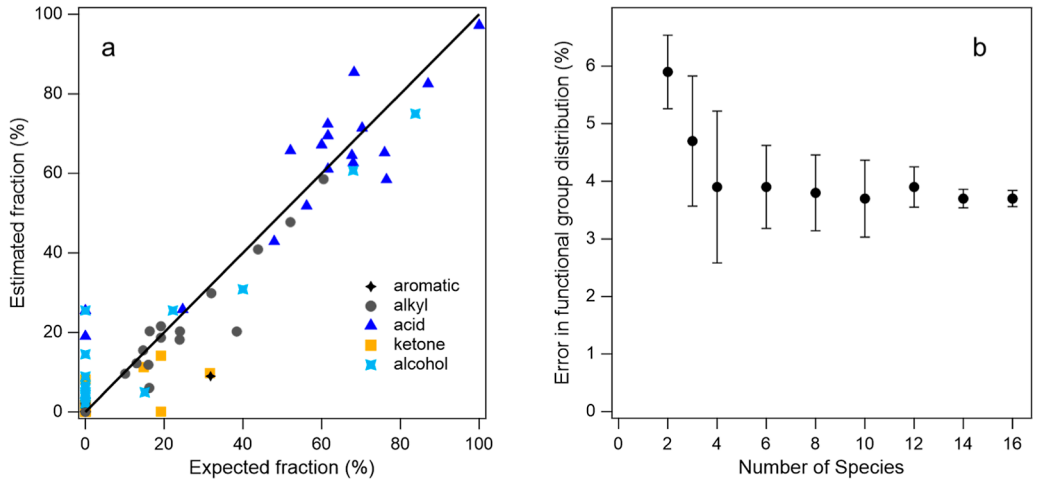

Figure 4. (a) Scatterplot between known weight fractions of the functional groups in the molecules and weight fractions estimated from AMS mass spectra. A 1:1 line is shown for reference. (b) Errors in the calculated functional group distribution compared to the known values as a function of the number of species in the mixture. Error bars are ±1 standard deviation across five different mixtures.

https://doi.org/10.1021/acsestair.6c00059
ACS EST Air 2026, 3, 1421−1434

of the weighting decisions for the overlapping ions is provided in Section S6.

A large portion of the signal for the oxidized fragments can be grouped using the delta analysis, but it does not include all the ions. Many AMS spectra have some ions containing three or more oxygen atoms. These must be from polyfunctional molecules, but the fragments will not follow a homologous series and thus are not included. Also, for the CHO_1 and CHO_2 ions in Figure 3a,b, intensities for ions with delta values less than -2Δ are not included in the current lists. Minimal signal is observed for these ions for most of the standards, with the largest signal from oxidized aromatics. Finally, we do not include CO^+ or the organic portion of water because these intensities are set based on the CO_2^+ signal. Overall, the analysis here uses about 92−99% of the total signal for these standards (excluding CO^+ and organic H_2O^+ fragments). Thus, the ions that are not included are a small fraction of the total ion signal. In the next sections we demonstrate application to the standards presented here as well as complex mixtures from combustion OA and PMF factors.

3.3. Functional Group Fractions of Standards

Following the methods described above, the fragment ions can be grouped by functional group and then the relative fraction of each functional group can be calculated. Figure 4a shows the relative weight fractions of five different functional groups calculated from the AMS spectra for these polyfunctional standards compared to the known functional group composition. The data for the acids, alcohols, and the alkyl groups generally cluster around the 1:1 line with lower estimates for some ketone and aromatic containing compounds. Overall, these standards show good correlations with the expected weight fractions with an average absolute error of about 5% and with a maximum observed absolute error of 26%.

For these calculations, as noted in Section 2.2, we assume that all functional groups are present. This is not true for all standards shown here, resulting in some false positive signals for alcohols and acids that can be seen as positive values for the estimated fractions with zero expected fractions. For the complex mixtures found in OA, it is more likely that al the functional groups will be present, decreasing the likelihood for false positives. The slope for the combined data sets is 0.92 and the R^2 is 0.91. The ketone-containing compounds that are underestimated have the ketone close to another oxidized group, resulting in decreased signal for CHO_1 ions at $+2\Delta$. In the future, this underprediction could be improved by attributing some portion of the CHO_3 ions to ketone groups. This will likely be based on the O/C of the sample, because the largest differences are seen for pyruvic acid and ketoglutaric acid, both of which have a high O/C and the carbonyl group right next to a carboxylic acid group. The aromatics are underestimated because there is overlap between aliphatic and aromatic compounds for CH fragments in the range of -2Δ to -6Δ, as noted above in Figure 3 and as seen in the standards in Figure 2. The data from Figure 4a is given in a table in the supplemental (Table S5).

The comparisons in Figure 4a are expected to have a larger error compared to a mixture where small inaccuracies can balance each other. This type of improvement was also observed for O/C estimates using these same standards.[35] Figure 4b shows improvement in the error when a mixture is analyzed compared to individual chemicals. To calculate this trend, different theoretical standard mixtures were generated by creating mixtures of standards with different numbers of species (e.g., x-axis on Figure 4b). The functional group contributions were then calculated from the theoretical AMS spectra of each of these mixtures and compared to expected fractions. The average error was calculated from the absolute value of the difference between the expected and the estimated fractions. Additional details on the method used here are provided at the end of Section S1.

Overall, there is scatter in the oxidized groups with a possible lower estimate for ketones and more false positives for alcohols and acids. In a mixture, these larger biases for individual chemicals should become less important. The data in Figure 4b show a decrease in error from around 6% to 4% when increasing the number of included species. The variability across the different sets of standards (i.e., the error bars) is also larger initially and decreases with higher numbers of species because there are more common chemicals between the runs. The average error plateaus at around 4% after only 4−6 species, similar to the trend observed for O/C estimates.[35] Given that OA is a mixture of thousands to tens of thousands of chemicals, we can expect an average error in the range of 4−6% in OA functional group fraction calculations.

The data shown in Figure 4 does not include three standards that contained esters. These were excluded because we find that esters form fragment ions that match acids and alcohols and are hence hard to distinguish and evaluate in a scatter plot. Figure S8 shows the relative functional group distributions for three ester compounds. It is likely that these compounds are fragmenting on the heater, leading to a decreased signal at $+4\Delta$ for CHO_2 fragments. Future work will target a wider range of oxidized esters to determine the relative weighting between acid and alcohol fragments. Because of the fragmentation on the heater, it will be challenging to quantify esters with the AMS and this is an area where comparisons with offline methods like FTIR and colorimetric methods could be beneficial.[10,18]

The standards used here do not contain chemicals with ether, peroxide, or amine groups. In GC/MS, the delta series for alcohols can also contain ethers and the delta series for acids also has esters.[24] Thus, we expect that ethers, peroxides, and esters will overlap with the existing functional groups, but more work is needed to determine how they compare to what has been found with GC/MS. Amines contain nitrogen and they follow the nitrogen rule which is described briefly in supplemental Section S7. Based on GC/MS data, amines should be found at $+1\Delta$ and $+3\Delta$, but the fragmentation of oxidized amines in the AMS needs to be evaluated. Organonitrates tend to fragment into inorganic ions NO_2^+ and NO^+, and methods of quantification have been developed.[39,40] A broader range of standards including ethers, peroxides, oxidized amines, and aromatics is a target for future studies.

3.4. Functional Group Fractions of OA Mixtures

Combustion of biomass and coal are important sources for OA in the atmosphere and in urban areas.[41−43] Functional group fractions have been previously calculated for combustion OA samples from wood and coal burning.[23] In this prior work, the peaks that corresponded to different functional groups were identified by comparison to FTIR data from filters collected concurrently with AMS measurements. The FTIR data was quantified for four different functional groups: alkyls, carboxylic acids, ketones, and alcohols. The AMS fragment

https://doi.org/10.1021/acsestair.6c00059
ACS EST Air 2026, 3, 1421−1434

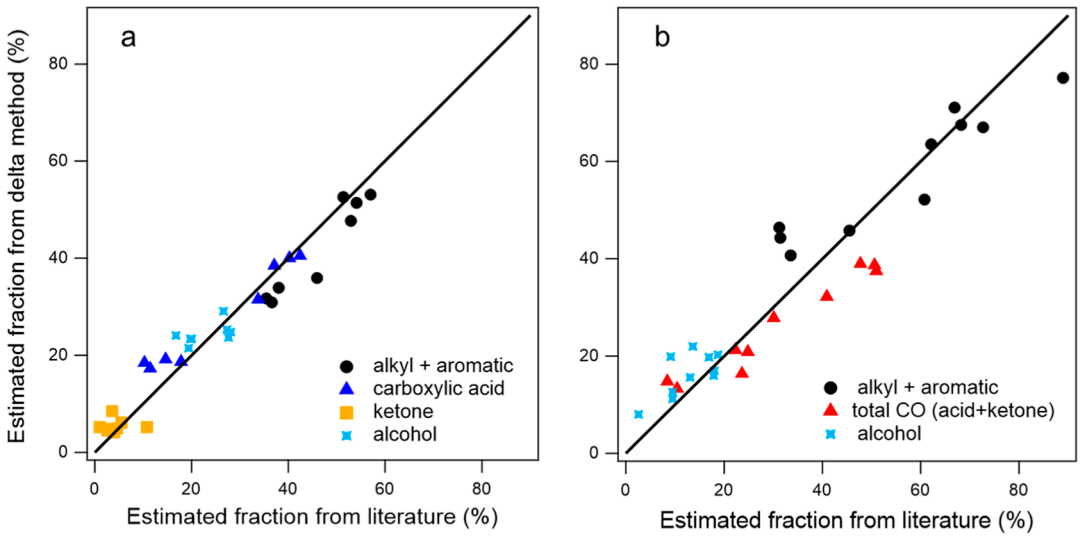

Figure 5. Scatterplot of functional group fractions from a study using FTIR compared to functional group fractions calculated using the delta method. (a) Wood combustion OA and (b) coal combustion OA. The functional groups are color coordinated and the acid and ketone fractions are combined in (b).

ions that correlated with these functional groups match some of the same ones used here for the delta functional group method, but others differed. For example, some CH-containing ions were assigned to acids in the FTIR study because they correlated with the acid signal for those data sets. However, those assignments will not necessarily extend to other OA samples. Thus, the work of Yazdani et al., (2022) demonstrates the ability for the AMS to quantify functional groups, but the method requires filter samples and offline FTIR analysis to identify the ions that correlate with the functional groups.

We have applied our functional group quantification to the AMS spectra from this study for the time points where direct comparisons were made with FTIR. Figure 5 shows a scatterplot of the measured functional group fractions for the delta analysis presented here compared to the estimates from the paper with combined AMS/FTIR analysis.[23] Both wood (Figure 5a) and coal (Figure 5b) combustion were measured before and after aging with oxidants. Since only alkyls were quantified in Yazdani et al., (2022) but all the AMS fragments were used for the statistical analysis, the aromatic and alkyl AMS fractions were also combined for our delta analysis. The correlation between the two methods is very good for the wood combustion (Figure 5a). The average error is 3% with a maximum observed error of 10%, which is in the range expected for an OA sample containing a complex mixture of chemicals. For Figure 5a, the slope was 0.86 with an R^2 of 0.94 and for Figure 5b the slope was 0.83 with an R^2 of 0.90. All errors are the absolute value of the difference between the delta estimates compared to the literature values.

For the coal combustion samples, the data is more complicated because some of the coal samples showed negative values for the carboxylic acids in the AMS/FTIR analysis.[23] This demonstrates either uncertainty in the quantification of the acids from the OH stretching region in the IR or challenges with comparisons between filter FTIR measurements vs AMS measurements of OA. Given the challenge of quantification in the bonded OH region, the total CO (acid + carbonyl) signal is likely more robust; this is compared in Figure 5b with an average error of 6% and with a maximum observed error of 15%. For these samples, some of the estimates for the alcohol fraction using delta analysis are a bit higher and some of the fractions of total CO are a bit lower compared to the FTIR fitted data. Looking at radial delta plots, there is an increase in signals in the CHO_1 region with delta values less than -2Δ for the aged samples relative to the unaged samples (Figure S9). These are likely oxidized aromatics because they have a high level of unsaturation. The functional groups for these CHO_1 ions at more negative delta values are not identified here because we lack standards to assign them. Their signal fraction is small, but they may be a source for some of the differences between the two methods in Figure 5b.

The comparison for the full data set from Figure 5b (alkyl, carboxylic acid, ketone, and alcohol) is provided in Figure S10. For the full data set, the delta functional group method shows a higher acid fraction and a lower carbonyl fraction (here ketones for delta) compared to the values from the AMS/FTIR correlation.[23] Larger spreads between the FTIR based values and the AMS delta estimates are observed for the aged/oxidized samples compared to the fresh coal combustion. From the standards, we know that ketones can be underpredicted with the delta method, especially when they are located right next to another functional group (Figure 4) and we are not able to quantify aldehydes, vide infra. However, the good overlap with the total CO shown in Figure 5b suggests that if the limitation here is the correct quantification of ketones, we would also have to be overpredicting the acid fraction by a similar amount. The difference between FTIR and AMS data was also observed in Yazdani et al., (2022). In that paper, they noted negative values for some of their acid and ketone predicted fractions in the AMS data. A similar gap between FTIR and AMS data sets was observed in the aromatic SOA factor in Bakersfield where the FTIR shows a small acid fraction but the AMS shows strong intensity at CO_2^+.[44] For both the coal combustion and the Bakersfield data sets, the FTIR C═O region does not show absorption consistent with esters. Future studies comparing these methods will be needed to fully explain the differences for the coal combustion data, but the good correlation with the well-established FTIR measurement for total CO suggests that both methods are capturing the overall trends in the functional groups well.

https://doi.org/10.1021/acsestair.6c00059
ACS EST Air 2026, 3, 1421−1434

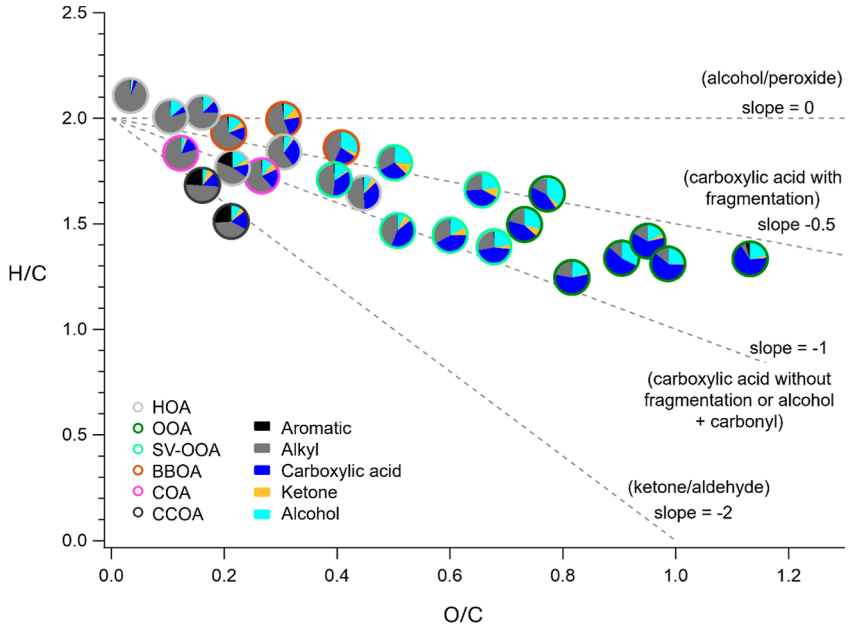

Figure 6. Van Krevelen diagram for the OA components from PMF factors from the literature. Pie charts show the fractions of the different functional groups and colored circles indicate the factor (HOA = hydrocarbon OA, OOA = the most oxidized factor, SV-OOA = the semivolatile-oxidized factor, BBOA = biomass burning OA, COA = cooking OA, CCOA = coal combustion OA. The pie charts cover, but are not perfectly centered on the data point for each factor. This was done to enable a visual intercomparison between nearby data sets.

In summary, the delta functional group analysis introduced here focuses on five functional groups quantified in OA: alkyls, aromatics, carboxylic acids, ketones, and alcohol groups. The comparison across these groups and FTIR data for OA samples is good with strong overlaps from a recent study looking at combustion OA (~3−6% average spread with a maximum of 15%). A greater spread is observed for the aged coal combustion (Figure S10) with the AMS reporting higher acid and lower ketone fractions compared to the FTIR. Here, the average spread was 6−8% for alkyl and alcohol and 19−20% for acid and ketone fractions with a maximum of 43%. More work is needed to determine if the difference is due to uncertainties in the bonded OH signal in FTIR for acid groups on aromatics or if improved constraints are needed for functional group estimates of oxidized aromatics in the AMS.

3.5. Functional Groups of PMF Factors

Several recent studies have examined ways to evaluate the aging and evolution of OA composition using elemental ratios and Van Krevelen diagrams.[45−47] Potential trends in oxidation/aging reactions were determined by looking at the slopes of O/C vs H/C ratios on the diagram. These reactions include the addition of carboxylic acids or hydroxy carbonyls without fragmentation (slope = −1) or the addition of alcohols (slope = 0) or of ketones/aldehydes (slope = −2). For OA from ambient and chamber studies, slopes between the −1 and the −0.5 line were reported, consistent with changes that correspond to the addition of acids with fragmentation and/or the addition of alcohols/peroxides and acids without fragmentation.[45]

Positive matrix factorization (PMF) is often applied to AMS data sets to characterize OA sources and composition as a function of time.[34,48] To probe potential differences in functional group distributions across ambient OA studies, we applied delta functional group analysis to PMF factors from the literature. Figure 6 shows the average functional group distributions for PMF factors from seven different field campaigns: Milagro,[49] Summer Beijing,[50] DUARE,[51] KORUS-AQ,[52] Changdo,[53] China,[54] and CARES.[55] Pie charts for the functional groups are given for each PMF factor, and the location on the Van Krevelen diagram is proportional to the O/C and H/C ratios calculated from the mass spectrum. The color surrounding the pie chart corresponds to the type of factor. For simplicity, we grouped all the more oxidized factors (darker green, labeled OOA) and the less oxidized factors (lighter green, labeled SV-OOA) together regardless of the name used in the publication. A complete list of the factors and the values is given in Table S6.

The data in Figure 6 generally falls between the −1 and −0.5 slopes with an apparent leveling off at higher O/C, consistent with prior studies.[45,46] The samples with the highest acid fraction are located in the far right and the samples with larger ketone fractions are generally observed in the middle of the O/C range. As noted above, the delta method can underpredict the ketone fraction for highly oxidized samples, so additional comparisons are needed to determine if the observed decrease in ketones at higher O/C is due to this underprediction. However, carbonyls are photoactive and studies have demonstrated a decrease in these functional groups with photolysis time,[56,57] so lower fractions in the more oxidized OA factors could be consistent with OA that has had the majority of carbonyls photobleached. The more oxidized OA factors may also come from sources with fewer ketone groups. The acid fraction from the delta analysis ranges from 4−67% with an average of 31% (not weighted by OA mass for the campaigns, Table S6). This average is similar to the average of 28% reported in Yatavelli et al., (2015).[58] The range here is wider than the range of 10−50% reported in Yatavelli et al., (2015), but we are evaluating PMF factors which can give greater separation between more and less oxidized OA.

Some differences are observed when comparing the functional groups to the trends expected based on the slopes on the diagram. For example, decreases along the −2 slope are

https://doi.org/10.1021/acsestair.6c00059
ACS EST Air 2026, 3, 1421−1434

not solely due to the addition of ketones. This can be seen in the upper left with factors that follow the −2 slope and have larger aromatic fractions, demonstrating that shifts in the H/C space can also come from different levels of unsaturation of the hydrocarbon fraction. In addition, the functional group distributions can be quite different despite the elemental ratios being close together in the Van Krevelen space. This happens because an alcohol plus a carbonyl is equivalent to an acid, so the relative fractions can vary without changing the O/C and H/C values. Examples of this can be seen across the different factor types and also within individual factors where a variety of different functional group distributions are observed. Different functional group distributions for samples with similar O/C and H/C ratios likely indicate a different source or very different aging pathways for the two aerosol populations.

Overall, the more oxidized factors generally show about a quarter of the mass as alcohol groups and a little more than half the mass as acid groups. If the trends shown in Figure 6 are representative of OA aging in the atmosphere, then more oxidized OA is showing some alcohol in addition to the carboxylic acids that have been previously highlighted as an important product of OA aging based on trends in f_{44}.[45] This functional group analysis provides a quantitative comparison of the differences across PMF factors from different locations. Future work should link the functional group trends with important physical properties of OA including volatility, hygroscopicity, and light absorption.

4. LIMITATIONS AND ATMOSPHERIC IMPLICATIONS

The work presented here demonstrates that estimates for five different functional groups can be made from AMS spectra using delta analysis. The measured O/C value is used to correct the relative fractions of oxidized vs nonoxidized groups and we have found only small corrections needed for the samples we have analyzed so far (±0.0−0.5 O/C units). The largest difference was observed for succinic acid and OA mixtures tend to show values at or below the average value for the standards, which is 0.2 O/C units. After this correction, all the oxidized fragments that are part of the O/C measurement are being attributed to alcohol, acid, and ketone groups. Future work will involve tracking the correction factor (x) across a wider range of standards to better understand processes like dehydration in the AMS. Signal for any other groups present in OA like esters, ethers, aldehydes, or peroxides are part of these groups (e.g., acid + ester instead of just acid). The standards used here suggest that esters will likely be contributing a large fraction of their signal to acids with some to alcohols (Figure S8). More work is needed to fully understand the fragmentation patterns for esters, ethers, aldehydes, and peroxides.

Aldehydes will be difficult to identify with the AMS as their thermal decomposition produces CO, which is not quantified in ambient AMS data sets due to the overlap in signal from N_2.[26,59] If an aldehyde undergoes EI, one of the main fragments is CHO^+, which is an important fragment in the AMS for alcohols. Given these challenges for aldehydes, we label the carbonyl fraction ketones and note that this will thus likely be an underestimate of the total carbonyl signal. It may be possible to study aldehyde fractions with offline-AMS using argon carrier gas or chamber studies with high loading.[60]

The radial delta plots also provide a rapid way to determine if substantial oxidized signal is present in the ranges that are not currently identified: CHO_1 ions less than -2Δ and CHO_2 ions less than 3Δ. Large signals for these ions were not observed for these standards, but an increase in these ions was observed for the coal combustion with aging (Figure S9). In future studies that look at a broader range of oxidized aromatics we will try to identify functional groups for these ions for OA relevant chemicals and further improve the quantification of the aromatic fraction.

Overall, both the radial delta plots and the functional group analysis described here will be helpful for comparisons across different AMS spectra, including enabling composition comparisons in the absence of long time-resolved data sets where positive matrix factorization (PMF) can be used.[48] One example of this is offline-AMS where extracts of individual filter samples are reatomized for analysis in the AMS.[61−63] A second example is aircraft measurements where a short period of time is spent in a plume.[64,65] A third example is ambient or laboratory experiments with rapidly changing conditions such as analysis of aerosol volatility using thermal denuders,[66] analysis of OA from a wave flume,[67] or indoor OA.[68−70]

The methods introduced here can also be applied to data sets collected as a function of time. AMS data sets have been used to measure OA sources,[48,71] compare ambient and chamber SOA formation and aging,[72−74] and understand oxidation mechanisms and OA loss processes.[75−77] In all these studies, elemental ratios measured with AMS have been a key component. The radial plots and the functional group analysis we describe here enables a deeper look into the assumptions and conclusions drawn from the AMS data sets. The results from a delta functional group analysis will also provide improved insights into the physical properties of OA. For example, OA volatility, viscosity, and hygroscopicity have been shown to depend on functional groups.[9,78,79] Thus, estimates of the relative fractions can be used to better constrain OA physical properties.

The functional group quantification method described here provides the first broadly applicable estimate of the functional group distribution in real-time OA data sets for the AMS. This method can be used to better understand OA sources and aging processes, and it may be used to better constrain properties like OA volatility and viscosity. The work discussed here is a foundation for future work. In subsequent publications, we will develop a similar functional group quantification method that can be applied to lower resolution data sets from the atmospheric chemical speciation monitor (ACSM). Here, we focus on C, H, and O containing fragments. Some ambient samples also contain nitrogen fragments, many of which are characteristic of the type of nitrogen functional groups in the samples. We will explore analysis of CHN and CHON delta plots and functional groups in future publications.

■ ASSOCIATED CONTENT

Supporting Information

The Supporting Information is available free of charge at https://pubs.acs.org/doi/10.1021/acsestair.6c00059.

(Section S1) Functional group fraction calculations, (Section S2) Additional delta plots of standards, (Section S3) Guidelines for interpreting delta plots, (Section S4) Demonstration of dehydration in AMS, (Section S5) Tables of common fragment ions in AMS spectra, (Section S6) Assigned ions and intensity

https://doi.org/10.1021/acsestair.6c00059
ACS EST Air 2026, 3, 1421−1434

weighting, (Section S7) Delta vs DBE and nitrogen containing compounds, (Section S8) Information on code to calculate delta plots and functional group distributions, (Table S5) Expected vs measured functional group fractions for standards, (Table S6) Elemental ratios and functional group content for PMF factors, (Figure S8) Relative fractions of functional groups for ester containing molecules, (Figure S9) Delta plots for coal combustion samples, (Figure S10) Scatterplot of coal combustion OA for all functional groups (PDF)

AUTHOR INFORMATION

Corresponding Author

Rachel E. O'Brien − *Department of Civil and Environmental Engineering, University of Michigan, Ann Arbor, Michigan 48105, United States;* orcid.org/0000-0001-8829-5517; Email: reobrien@umich.edu

Authors

Manjula Canagaratna − *Aerodyne Research, Inc., Billerica, Massachusetts 01821, United States*

Xu He − *Department of Civil and Environmental Engineering, University of Michigan, Ann Arbor, Michigan 48105, United States*

Yeaseul Kim − *Department of Civil and Environmental Engineering, University of Michigan, Ann Arbor, Michigan 48105, United States*

Adam Nix − *Department of Civil and Environmental Engineering, University of Michigan, Ann Arbor, Michigan 48105, United States*

Hannah S. Kenagy − *Department of Chemistry, University of Minnesota, Minneapolis, Minnesota 55455, United States;* orcid.org/0000-0002-0096-530X

Complete contact information is available at: https://pubs.acs.org/10.1021/acsestair.6c00059

Notes

The authors declare no competing financial interest.

ACKNOWLEDGMENTS

This work is supported by the Department of Energy DOE grant DE-SC0025197 and National Oceanic and Atmospheric Administration (Atmospheric Chemistry, Carbon Cycle, and climate Program, Climate Program) grants NA21OAR4310135-T1-01, NA23OAR4310293. H.S.K. acknowledges funding from UMN Department of Chemistry.

REFERENCES

(1) Masson-Delmotte, V., Zhai, P., Pirani, A., Connors, S. L., Péan, C., Berger, S., Caud, N., Chen, Y., Goldfarb, L., Gomis, M. I., Huang, M., Leitzell, K., Lonnoy, E., Matthews, J. B. R., Maycock, T. K., Waterfield, T., Yelekçi, O., Yu, R., Zhou, B.. *IPCC, 2021: Climate Change 2021: The Physical Science Basis. Contribution of Working Group I to the Sixth Assessment Report of the Intergovernmental Panel on Climate Change*, Eds.; Cambridge University Press: Cambridge, United Kingdom and New York, NY, USA, 2023.

(2) Pope, C. A.; Dockery, D. W. Health Effects of Fine Particulate Air Pollution: Lines That Connect. *J. Air Waste Manage. Assoc.* **2006**, *56* (6), 709−742.

(3) Zhang, Q.; Jimenez, J. L.; Canagaratna, M. R.; Allan, J. D.; Coe, H.; Ulbrich, I.; Alfarra, M. R.; Takami, A.; Middlebrook, A. M.; Sun, Y. L.; Dzepina, K.; Dunlea, E.; Docherty, K.; DeCarlo, P. F.; Salcedo, D.; Onasch, T.; Jayne, J. T.; Miyoshi, T.; Shimono, A.; Hatakeyama, S.; Takegawa, N.; Kondo, Y.; Schneider, J.; Drewnick, F.; Borrmann, S.; Weimer, S.; Demerjian, K.; Williams, P.; Bower, K.; Bahreini, R.; Cottrell, L.; Griffin, R. J.; Rautiainen, J.; Sun, J. Y.; Zhang, Y. M.; Worsnop, D. R. Ubiquity and Dominance of Oxygenated Species in Organic Aerosols in Anthropogenically-Influenced Northern Hemisphere Midlatitudes. *Geophys. Res. Lett.* **2007**, *34* (13), 1−6.

(4) Goldstein, A. H.; Galbally, I. E. Known and Unexplored Organic Constituents in the Earth's Atmosphere. *Environ. Sci. Technol.* **2007**, *41* (5), 1514−1521.

(5) Hamilton, J. F. Using Comprehensive Two-Dimensional Gas Chromatography to Study the Atmosphere. *J. Chromatogr. Sci.* **2010**, *48* (4), 274−282.

(6) Donahue, N. M.; Epstein, S. A.; Pandis, S. N.; Robinson, A. L. A Two-Dimensional Volatility Basis Set: 1. Organic-Aerosol Mixing Thermodynamics. *Atmos. Chem. Phys.* **2011**, *11* (7), 3303−3318.

(7) Grayson, J. W.; Evoy, E.; Song, M.; Chu, Y.; Maclean, A.; Nguyen, A.; Upshur, M. A.; Ebrahimi, M.; Chan, C. K.; Geiger, F. M.; Thomson, R. J.; Bertram, A. K. The Effect of Hydroxyl Functional Groups and Molar Mass on the Viscosity of Non-Crystalline Organic and Organic−Water Particles. *Atmos. Chem. Phys.* **2017**, *17* (13), 8509−8524.

(8) Shiraiwa, M.; Li, Y.; Tsimpidi, A. P.; Karydis, V. A.; Berkemeier, T.; Pandis, S. N.; Lelieveld, J.; Koop, T.; Pöschl, U. Global Distribution of Particle Phase State in Atmospheric Secondary Organic Aerosols. *Nat. Commun.* **2017**, *8* (1), 15002.

(9) Suda, S. R.; Petters, M. D.; Yeh, G. K.; Strollo, C.; Matsunaga, A.; Faulhaber, A.; Ziemann, P. J.; Prenni, A. J.; Carrico, C. M.; Sullivan, R. C.; Kreidenweis, S. M. Influence of Functional Groups on Organic Aerosol Cloud Condensation Nucleus Activity. *Environ. Sci. Technol.* **2014**, *48* (17), 10182−10190.

(10) Coury, C.; Dillner, A. M. A Method to Quantify Organic Functional Groups and Inorganic Compounds in Ambient Aerosols Using Attenuated Total Reflectance FTIR Spectroscopy and Multivariate Chemometric Techniques. *Atmos. Environ.* **2008**, *42* (23), 5923−5932.

(11) Kidd, C.; Perraud, V.; Wingen, L. M.; Finlayson-Pitts, B. J. Integrating Phase and Composition of Secondary Organic Aerosol from the Ozonolysis of α-Pinene. *Proc. Natl. Acad. Sci. U.S.A.* **2014**, *111* (21), 7552−7557.

(12) Mei, S.; Xia, K.; Liu, C.; Chen, X.; Yuan, R.; Liu, H.; Zhao, C.; Liu, S. Aqueous-Phase Processing Affects the Formation and Size Distribution of Aerosol Organic Functional Groups During Heavy Pollution. *JGR Atmospheres* **2025**, *130* (3), No. e2024JD042029.

(13) Russell, L. M.; Bahadur, R.; Hawkins, L. N.; Allan, J.; Baumgardner, D.; Quinn, P. K.; Bates, T. S. Organic Aerosol Characterization by Complementary Measurements of Chemical Bonds and Molecular Fragments. *Atmos. Environ.* **2009**, *43* (38), 6100−6105.

(14) Decesari, S.; Mircea, M.; Cavalli, F.; Fuzzi, S.; Moretti, F.; Tagliavini, E.; Facchini, M. C. Source Attribution of Water-Soluble Organic Aerosol by Nuclear Magnetic Resonance Spectroscopy. *Environ. Sci. Technol.* **2007**, *41* (7), 2479−2484.

(15) Tagliavini, E.; Moretti, F.; Decesari, S.; Facchini, M. C.; Fuzzi, S.; Maenhaut, W. Functional Group Analysis by H NMR/Chemical Derivatization for the Characterization of Organic Aerosol from the SMOCC FIeld Campaign. *Atmos. Chem. Phys.* **2006**.

(16) Ditto, J. C.; Machesky, J.; Gentner, D. R. Analysis of Reduced and Oxidized Nitrogen-Containing Organic Compounds at a Coastal Site in Summer and Winter. *Atmos. Chem. Phys.* **2022**, *22* (5), 3045−3065.

(17) El Haddad, I.; Marchand, N.; D'Anna, B.; Jaffrezo, J. L.; Wortham, H. Functional Group Composition of Organic Aerosol from Combustion Emissions and Secondary Processes at Two Contrasted Urban Environments. *Atmos. Environ.* **2013**, *75*, 308−320.

(18) Aimanant, S.; Ziemann, P. J. Development of Spectrophotometric Methods for the Analysis of Functional Groups in Oxidized Organic Aerosol. *Aerosol Sci. Technol.* **2013**, *47* (6), 581−591.

(19) Canagaratna, M. R.; Jayne, J. T.; Jimenez, J. L.; Allan, J. D.; Alfarra, M. R.; Zhang, Q.; Onasch, T. B.; Drewnick, F.; Coe, H.; Middlebrook, A.; Delia, A.; Williams, L. R.; Trimborn, A. M.; Northway, M. J.; DeCarlo, P. F.; Kolb, C. E.; Davidovits, P.; Worsnop, D. R. Chemical and Microphysical Characterization of Ambient Aerosols with the Aerodyne Aerosol Mass Spectrometer. *Mass Spectrom. Rev.* **2007**, *26* (2), 185−222.
(20) DeCarlo, P. F.; Kimmel, J. R.; Trimborn, A.; Northway, M. J.; Jayne, J. T.; Aiken, A. C.; Gonin, M.; Fuhrer, K.; Horvath, T.; Docherty, K. S.; Worsnop, D. R.; Jimenez, J. L. Field-Deployable, High-Resolution, Time-of-Flight Aerosol Mass Spectrometer. *Anal. Chem.* **2006**, *78* (24), 8281−8289.
(21) Chen, Q.; Ikemori, F.; Higo, H.; Asakawa, D.; Mochida, M. Chemical Structural Characteristics of HULIS and Other Fractionated Organic Matter in Urban Aerosols: Results from Mass Spectral and FT-IR Analysis. *Environ. Sci. Technol.* **2016**, *50* (4), 1721−1730.
(22) Faber, P.; Drewnick, F.; Bierl, R.; Borrmann, S. Complementary Online Aerosol Mass Spectrometry and Offline FT-IR Spectroscopy Measurements: Prospects and Challenges for the Analysis of Anthropogenic Aerosol Particle Emissions. *Atmos. Environ.* **2017**, *166*, 92−98.
(23) Yazdani, A.; Dudani, N.; Takahama, S.; Bertrand, A.; Prévôt, A. S. H.; El Haddad, I.; Dillner, A. M. Fragment Ion−Functional Group Relationships in Organic Aerosols Using Aerosol Mass Spectrometry and Mid-Infrared Spectroscopy. *Atmos. Meas. Technol.* **2022**, *15* (9), 2857−2874.
(24) McLafferty, F.; Turecek, F. *Interpretation of Mass Spectra*; Fourth; University Science Books, 1993.
(25) Isaacman, G.; Kreisberg, N. M.; Yee, L. D.; Worton, D. R.; Chan, A. W. H.; Moss, J. A.; Hering, S. V.; Goldstein, A. H. Online Derivatization for Hourly Measurements of Gas- and Particle-Phase Semi-Volatile Oxygenated Organic Compounds by Thermal Desorption Aerosol Gas Chromatography (SV-TAG). *Atmos. Meas. Technol.* **2014**, *7* (12), 4417−4429.
(26) Moldoveanu, S. *Pyrolysis of Organic Molecules: Applications to Health and Environmental Issues*; Elsevier Science, 2009.
(27) Alfarra, M. R. Insights into Atmospheric Organic Aerosols Using an Aerosol Mass Spectrometer; PhD Thesis: Manchester, UK, 2004..
(28) Schneider, J.; Weimer, S.; Drewnick, F.; Borrmann, S.; Helas, G.; Gwaze, P.; Schmid, O.; Andreae, M. O.; Kirchner, U. Mass Spectrometric Analysis and Aerodynamic Properties of Various Types of Combustion-Related Aerosol Particles. *Int. J. Mass Spectrom.* **2006**, *258* (1−3), 37−49.
(29) Dromey, R. G. Simple Index for Classifying Mass Spectra with Applications to Fast Library Searching. *Anal. Chem.* **1976**, *48* (11), 1464−1469.
(30) Bahreini, R.; Keywood, M. D.; Ng, N. L.; Varutbangkul, V.; Gao, S.; Flagan, R. C.; Seinfeld, J. H.; Worsnop, D. R.; Jimenez, J. L. Measurements of Secondary Organic Aerosol from Oxidation of Cycloalkenes, Terpenes, and *m* -Xylene Using an Aerodyne Aerosol Mass Spectrometer. *Environ. Sci. Technol.* **2005**, *39* (15), 5674−5688.
(31) Kroll, J. H.; Smith, J. D.; Worsnop, D. R.; Wilson, K. R. Characterisation of Lightly Oxidised Organic Aerosol Formed from the Photochemical Aging of Diesel Exhaust Particles. *Environ. Chem.* **2012**, *9* (3), 211.
(32) Ugelow, M. S.; Zarzana, K. J.; Day, D. A.; Jimenez, J. L.; Tolbert, M. A. The Optical and Chemical Properties of Discharge Generated Organic Haze Using In-Situ Real-Time Techniques. *Icarus* **2017**, *294*, 1−13.
(33) Ulbrich, I. M.; Handschy, A. V.; Lechner, M. J.; Jimenez, J. L. High-Resolution AMS Spectral Database. https://cires1.colorado.edu/jimenez-group/HRAMSsd/(accessed Mar 10, 2025).
(34) Ulbrich, I. M.; Canagaratna, M. R.; Zhang, Q.; Worsnop, D. R.; Jimenez, J. L. Interpretation of Organic Components from Positive Matrix Factorization of Aerosol Mass Spectrometric Data. *Atmos. Chem. Phys.* **2009**.
(35) Canagaratna, M. R.; Jimenez, J. L.; Kroll, J. H.; Chen, Q.; Kessler, S. H.; Massoli, P.; Hildebrandt Ruiz, L.; Fortner, E.; Williams, L. R.; Wilson, K. R.; Surratt, J. D.; Donahue, N. M.; Jayne, J. T.; Worsnop, D. R. Elemental Ratio Measurements of Organic Compounds Using Aerosol Mass Spectrometry: Characterization, Improved Calibration, and Implications. *Atmos. Chem. Phys.* **2015**, *15* (1), 253−272.
(36) Jeon, S.; Walker, M. J.; Sueper, D. T.; Day, D. A.; Handschy, A. V.; Jimenez, J. L.; Williams, B. J. A Searchable Database and Mass Spectral Comparison Tool for the Aerosol Mass Spectrometer (AMS) and the Aerosol Chemical Speciation Monitor (ACSM). *Atmos. Meas. Technol.* **2023**, *16* (24), 6075−6095.
(37) Schneider, J.; Freutel, F.; Zorn, S. R.; Chen, Q.; Farmer, D. K.; Jimenez, J. L.; Martin, S. T.; Artaxo, P.; Wiedensohler, A.; Borrmann, S. Mass-Spectrometric Identification of Primary Biological Particle Markers and Application to Pristine Submicron Aerosol Measurements in Amazonia. *Atmos. Chem. Phys.* **2011**, *11* (22), 11415−11429.
(38) Cubison, M. J.; Ortega, A. M.; Hayes, P. L.; Farmer, D. K.; Day, D.; Lechner, M. J.; Brune, W. H.; Apel, E.; Diskin, G. S.; Fisher, J. A.; Fuelberg, H. E.; Hecobian, A.; Knapp, D. J.; Mikoviny, T.; Riemer, D.; Sachse, G. W.; Sessions, W.; Weber, R. J.; Weinheimer, A. J.; Wisthaler, A.; Jimenez, J. L. Effects of Aging on Organic Aerosol from Open Biomass Burning Smoke in Aircraft and Laboratory Studies. *Atmos. Chem. Phys.* **2011**, *11* (23), 12049−12064.
(39) Farmer, D. K.; Matsunaga, A.; Docherty, K. S.; Surratt, J. D.; Seinfeld, J. H.; Ziemann, P. J.; Jimenez, J. L.; Finlayson-Pitts, B. J. Response of an Aerosol Mass Spectrometer to Organonitrates and Organosulfates and Implications for Atmospheric Chemistry. *Proc. Natl. Acad. Sci. U.S.A.* **2010**, *107* (15), 6670−6675.
(40) Xu, L.; Suresh, S.; Guo, H.; Weber, R. J.; Ng, N. L. Aerosol Characterization over the Southeastern United States Using High-Resolution Aerosol Mass Spectrometry: Spatial and Seasonal Variation of Aerosol Composition and Sources with a Focus on Organic Nitrates. *Atmos. Chem. Phys.* **2015**, *15* (13), 7307−7336.
(41) Andreae, M. O. Emission of Trace Gases and Aerosols from Biomass Burning − an Updated Assessment. *Atmos. Chem. Phys.* **2019**.
(42) Haque, Md. M.; Kawamura, K.; Deshmukh, D. K.; Fang, C.; Song, W.; Mengying, B.; Zhang, Y.-L. Characterization of Organic Aerosols from a Chinese Megacity during Winter: Predominance of Fossil Fuel Combustion. *Atmos. Chem. Phys.* **2019**, *19* (7), 5147−5164.
(43) Jathar, S. H.; Gordon, T. D.; Hennigan, C. J.; Pye, H. O. T.; Pouliot, G.; Adams, P. J.; Donahue, N. M.; Robinson, A. L. Unspeciated Organic Emissions from Combustion Sources and Their Influence on the Secondary Organic Aerosol Budget in the United States. *Proc. Natl. Acad. Sci. U.S.A.* **2014**, *111* (29), 10473−10478.
(44) Liu, S.; Ahlm, L.; Day, D. A.; Russell, L. M.; Zhao, Y.; Gentner, D. R.; Weber, R. J.; Goldstein, A. H.; Jaoui, M.; Offenberg, J. H.; Kleindienst, T. E.; Rubitschun, C.; Surratt, J. D.; Sheesley, R. J.; Scheller, S. Secondary Organic Aerosol Formation from Fossil Fuel Sources Contribute Majority of Summertime Organic Mass at Bakersfield. *J. Geophys. Res.* **2012**, *117* (D24), 2012JD018170.
(45) Ng, N. L.; Canagaratna, M. R.; Jimenez, J. L.; Chhabra, P. S.; Seinfeld, J. H.; Worsnop, D. R. Changes in Organic Aerosol Composition with Aging Inferred from Aerosol Mass Spectra. *Atmos. Chem. Phys.* **2011**, *11* (13), 6465−6474.
(46) Heald, C. L.; Kroll, J. H.; Jimenez, J. L.; Docherty, K. S.; DeCarlo, P. F.; Aiken, A. C.; Chen, Q.; Martin, S. T.; Farmer, D. K.; Artaxo, P. A Simplified Description of the Evolution of Organic Aerosol Composition in the Atmosphere. *Geophys. Res. Lett.* **2010**, *37* (8), 2010GL042737.
(47) Chen, Q.; Heald, C. L.; Jimenez, J. L.; Canagaratna, M. R.; Zhang, Q.; He, L.; Huang, X.; Campuzano-Jost, P.; Palm, B. B.; Poulain, L.; Kuwata, M.; Martin, S. T.; Abbatt, J. P. D.; Lee, A. K. Y.; Liggio, J. Elemental Composition of Organic Aerosol: The Gap between Ambient and Laboratory Measurements. *Geophys. Res. Lett.* **2015**, *42* (10), 4182−4189.
(48) Zhang, Q.; Jimenez, J. L.; Canagaratna, M. R.; Ulbrich, I. M.; Ng, N. L.; Worsnop, D. R.; Sun, Y. Understanding Atmospheric

Organic Aerosols via Factor Analysis of Aerosol Mass Spectrometry: A Review. *Anal. Bioanal. Chem.* **2011**, *401* (10), 3045−3067.
(49) Aiken, A. C.; Salcedo, D.; Cubison, M. J.; Huffman, J. A.; DeCarlo, P. F.; Ulbrich, I. M.; Docherty, K. S.; Sueper, D.; Kimmel, J. R.; Worsnop, D. R.; Trimborn, A.; Northway, M.; Stone, E. A.; Schauer, J. J.; Volkamer, R. M.; Fortner, E.; de Foy, B.; Wang, J.; Laskin, A.; Shutthanandan, V.; Zheng, J.; Zhang, R.; Gaffney, J.; Marley, N. A.; Paredes-Miranda, G.; Arnott, W. P.; Molina, L. T.; Sosa, G.; Jimenez, J. L. Mexico City Aerosol Analysis during MILAGRO Using High Resolution Aerosol Mass Spectrometry at the Urban Supersite (T0) − Part 1: Fine Particle Composition and Organic Source Apportionment. *Atmos. Chem. Phys.* **2009**, 5315−5341.
(50) Hu, W.; Hu, M.; Hu, W.; Jimenez, J. L.; Yuan, B.; Chen, W.; Wang, M.; Wu, Y.; Chen, C.; Wang, Z.; Peng, J.; Zeng, L.; Shao, M. Chemical Composition, Sources, and Aging Process of Submicron Aerosols in Beijing: Contrast between Summer and Winter. *JGR Atmospheres* **2016**, *121* (4), 1955−1977.
(51) Mohr, C.; DeCarlo, P. F.; Heringa, M. F.; Chirico, R.; Slowik, J. G.; Richter, R.; Reche, C.; Alastuey, A.; Querol, X.; Seco, R.; Peñuelas, J.; Jiménez, J. L.; Crippa, M.; Zimmermann, R.; Baltensperger, U.; Prévôt, A. S. H. Identification and Quantification of Organic Aerosol from Cooking and Other Sources in Barcelona Using Aerosol Mass Spectrometer Data. *Atmos. Chem. Phys.* **2012**, *12* (4), 1649−1665.
(52) Hu, W.; Day, D. A.; Campuzano-Jost, P.; Nault, B. A.; Park, T.; Lee, T.; Croteau, P.; Canagaratna, M. R.; Jayne, J. T.; Worsnop, D. R.; Jimenez, J. L. Evaluation of the New Capture Vaporizer for Aerosol Mass Spectrometers (AMS): Elemental Composition and Source Apportionment of Organic Aerosols (OA). *ACS Earth Space Chem.* **2018**, *2* (4), 410−421.
(53) Hu, W. W.; Hu, M.; Yuan, B.; Jimenez, J. L.; Tang, Q.; Peng, J. F.; Hu, W.; Shao, M.; Wang, M.; Zeng, L. M.; Wu, Y. S.; Gong, Z. H.; Huang, X. F.; He, L. Y. Insights on Organic Aerosol Aging and the Influence of Coal Combustion at a Regional Receptor Site of Central Eastern China. *Atmos. Chem. Phys.* **2013**, *13* (19), 10095−10112.
(54) Elser, M.; Huang, R.-J.; Wolf, R.; Slowik, J. G.; Wang, Q.; Canonaco, F.; Li, G.; Bozzetti, C.; Daellenbach, K. R.; Huang, Y.; Zhang, R.; Li, Z.; Cao, J.; Baltensperger, U.; El-Haddad, I.; Prévôt, A. S. H. New Insights into PM2.5 Chemical Composition and Sources in Two Major Cities in China during Extreme Haze Events Using Aerosol Mass Spectrometry. *Atmos. Chem. Phys.* **2016**, *16* (5), 3207−3225.
(55) Setyan, A.; Zhang, Q.; Merkel, M.; Knighton, W. B.; Sun, Y.; Song, C.; Shilling, J. E.; Onasch, T. B.; Herndon, S. C.; Worsnop, D. R.; Fast, J. D.; Zaveri, R. A.; Berg, L. K.; Wiedensohler, A.; Flowers, B. A.; Dubey, M. K.; Subramanian, R. Characterization of Submicron Particles Influenced by Mixed Biogenic and Anthropogenic Emissions Using High-Resolution Aerosol Mass Spectrometry: Results from CARES. *Atmos. Chem. Phys.* **2012**, *12* (17), 8131−8156.
(56) Baboomian, V. J.; Gu, Y.; Nizkorodov, S. A. Photodegradation of Secondary Organic Aerosols by Long-Term Exposure to Solar Actinic Radiation. *ACS Earth Space Chem.* **2020**, *4* (7), 1078−1089.
(57) Walhout, E. Q.; Yu, H.; Thrasher, C.; Shusterman, J. M.; O'Brien, R. E. Effects of Photolysis on the Chemical and Optical Properties of Secondary Organic Material Over Extended Time Scales. *ACS Earth Space Chem.* **2019**, *3* (7), 1226−1236.
(58) Yatavelli, R. L. N.; Mohr, C.; Stark, H.; Day, D. A.; Thompson, S. L.; Lopez-Hilfiker, F. D.; Campuzano-Jost, P.; Palm, B. B.; Vogel, A. L.; Hoffmann, T.; Heikkinen, L.; Äijälä, M.; Ng, N. L.; Kimmel, J. R.; Canagaratna, M. R.; Ehn, M.; Junninen, H.; Cubison, M. J.; Petäjä, T.; Kulmala, M.; Jayne, J. T.; Worsnop, D. R.; Jimenez, J. L. Estimating the Contribution of Organic Acids to Northern Hemispheric Continental Organic Aerosol. *Geophys. Res. Lett.* **2015**, *42* (14), 6084−6090.
(59) Aiken, A. C.; DeCarlo, P. F.; Jimenez, J. L. Elemental Analysis of Organic Species with Electron Ionization High-Resolution Mass Spectrometry. *Anal. Chem.* **2007**, *79* (21), 8350−8358.
(60) Chhabra, P. S.; Flagan, R. C.; Seinfeld, J. H. Elemental Analysis of Chamber Organic Aerosol Using an Aerodyne High-Resolution Aerosol Mass Spectrometer. *Atmos. Chem. Phys.* **2010**, *10* (9), 4111−4131.
(61) Khare, P.; Kurdieh, A. A.; Hao, Y.; Manousakas, M.-I.; Dada, L.; Tobler, A.; Schneider-Beltran, K.; Diapouli, E.; Skiba, A.; Styszko, K.; Slowik, J. G.; Prévôt, A. S. H.; Daellenbach, K. R. Organic Solvents-Based Offline Aerosol Mass Spectrometry (SOff-AMS) for Comprehensive Chemical Characterization of Ambient Organic Aerosol. *Environ. Sci. Technol.* **2025**, *59* (34), 18236−18248.
(62) Niedek, C. R.; Mei, F.; Zawadowicz, M. A.; Zhu, Z.; Schmid, B.; Zhang, Q. Quantitative Chemical Assay of Nanogram-Level Particulate Matter Using Aerosol Mass Spectrometry: Characterization of Particles Collected from Uncrewed Atmospheric Measurement Platforms. *Atmos. Meas. Technol.* **2023**, *16* (4), 955−968.
(63) O'Brien, R. E.; Ridley, K. J.; Canagaratna, M. R.; Jayne, J. T.; Croteau, P. L.; Worsnop, D. R.; Budisulistiorini, S. H.; Surratt, J. D.; Follett, C. L.; Repeta, D. J.; Kroll, J. H. Ultrasonic Nebulization for the Elemental Analysis of Microgram-Level Samples with Offline Aerosol Mass Spectrometry. *Atmos. Meas. Technol.* **2019**, *12* (3), 1659−1671.
(64) Garofalo, L. A.; Pothier, M. A.; Levin, E. J. T.; Campos, T.; Kreidenweis, S. M.; Farmer, D. K. Emission and Evolution of Submicron Organic Aerosol in Smoke from Wildfires in the Western United States. *ACS Earth Space Chem.* **2019**, *3* (7), 1237−1247.
(65) Palm, B. B.; Peng, Q.; Fredrickson, C. D.; Lee, B. H.; Garofalo, L. A.; Pothier, M. A.; Kreidenweis, S. M.; Farmer, D. K.; Pokhrel, R. P.; Shen, Y.; Murphy, S. M.; Permar, W.; Hu, L.; Campos, T. L.; Hall, S. R.; Ullmann, K.; Zhang, X.; Flocke, F.; Fischer, E. V.; Thornton, J. A. Quantification of Organic Aerosol and Brown Carbon Evolution in Fresh Wildfire Plumes. *Proc. Natl. Acad. Sci. U.S.A.* **2020**, *117* (47), 29469−29477.
(66) Feng, T.; Wang, Y.; Hu, W.; Zhu, M.; Song, W.; Chen, W.; Sang, Y.; Fang, Z.; Deng, W.; Fang, H.; Yu, X.; Wu, C.; Yuan, B.; Huang, S.; Shao, M.; Huang, X.; He, L.; Lee, Y. R.; Huey, L. G.; Canonaco, F.; Prevot, A. S. H.; Wang, X. Impact of Aging on the Sources, Volatility, and Viscosity of Organic Aerosols in Chinese Outflows. *Atmos. Chem. Phys.* **2023**, *23* (1), 611−636.
(67) Wang, X.; Sultana, C. M.; Trueblood, J.; Hill, T. C. J.; Malfatti, F.; Lee, C.; Laskina, O.; Moore, K. A.; Beall, C. M.; McCluskey, C. S.; Cornwell, G. C.; Zhou, Y.; Cox, J. L.; Pendergraft, M. A.; Santander, M. V.; Bertram, T. H.; Cappa, C. D.; Azam, F.; DeMott, P. J.; Grassian, V. H.; Prather, K. A. Microbial Control of Sea Spray Aerosol Composition: A Tale of Two Blooms. *ACS Cent. Sci.* **2015**, *1* (3), 124−131.
(68) Farmer, D. K.; Vance, M. E.; Abbatt, J. P. D.; Abeleira, A.; Alves, M. R.; Arata, C.; Boedicker, E.; Bourne, S.; Cardoso-Saldaña, F.; Corsi, R.; DeCarlo, P. F.; Goldstein, A. H.; Grassian, V. H.; Hildebrandt Ruiz, L.; Jimenez, J. L.; Kahan, T. F.; Katz, E. F.; Mattila, J. M.; Nazaroff, W. W.; Novoselac, A.; O'Brien, R. E.; Or, V. W.; Patel, S.; Sankhyan, S.; Stevens, P. S.; Tian, Y.; Wade, M.; Wang, C.; Zhou, S.; Zhou, Y. Overview of HOMEChem: House Observations of Microbial and Environmental Chemistry. *Environ. Sci.: Processes Impacts* **2019**, *21* (8), 1280−1300.
(69) Katz, E. F.; Guo, H.; Campuzano-Jost, P.; Day, D. A.; Brown, W. L.; Boedicker, E.; Pothier, M.; Lunderberg, D. M.; Patel, S.; Patel, K.; Hayes, P. L.; Avery, A.; Hildebrandt Ruiz, L.; Goldstein, A. H.; Vance, M. E.; Farmer, D. K.; Jimenez, J. L.; DeCarlo, P. F. Quantification of Cooking Organic Aerosol in the Indoor Environment Using Aerodyne Aerosol Mass Spectrometers. *Aerosol Sci. Technol.* **2021**, *55* (10), 1099−1114.
(70) Omelekhina, Y.; Eriksson, A.; Canonaco, F.; Prevot, A. S. H.; Nilsson, P.; Isaxon, C.; Pagels, J.; Wierzbicka, A. Cooking and Electronic Cigarettes Leading to Large Differences between Indoor and Outdoor Particle Composition and Concentration Measured by Aerosol Mass Spectrometry. *Environ. Sci.: Processes Impacts* **2020**, *22* (6), 1382−1396.
(71) Crippa, M.; Canonaco, F.; Lanz, V. A.; Äijälä, M.; Allan, J. D.; Carbone, S.; Capes, G.; Ceburnis, D.; Dall'Osto, M.; Day, D. A.;

https://doi.org/10.1021/acsestair.6c00059
ACS EST Air 2026, 3, 1421−1434

DeCarlo, P. F.; Ehn, M.; Eriksson, A.; Freney, E.; Hildebrandt Ruiz, L.; Hillamo, R.; Jimenez, J. L.; Junninen, H.; Kiendler-Scharr, A.; Kortelainen, A.-M.; Kulmala, M.; Laaksonen, A.; Mensah, A. A.; Mohr, C.; Nemitz, E.; O'Dowd, C.; Ovadnevaite, J.; Pandis, S. N.; Petäjä, T.; Poulain, L.; Saarikoski, S.; Sellegri, K.; Swietlicki, E.; Tiitta, P.; Worsnop, D. R.; Baltensperger, U.; Prévôt, A. S. H. Organic Aerosol Components Derived from 25 AMS Data Sets across Europe Using a Consistent ME-2 Based Source Apportionment Approach. *Atmos. Chem. Phys.* **2014**, *14* (12), 6159−6176.

(72) Chhabra, P. S.; Ng, N. L.; Canagaratna, M. R.; Corrigan, A. L.; Russell, L. M.; Worsnop, D. R.; Flagan, R. C.; Seinfeld, J. H. Elemental Composition and Oxidation of Chamber Organic Aerosol. *Atmos. Chem. Phys.* **2011**, *11* (17), 8827−8845.

(73) Kenagy, H. S.; Heald, C. L.; Tahsini, N.; Goss, M. B.; Kroll, J. H. Can We Achieve Atmospheric Chemical Environments in the Laboratory? An Integrated Model-Measurement Approach to Chamber SOA Studies. *Sci. Adv.* **2024**.

(74) Porter, W. C.; Jimenez, J. L.; Barsanti, K. C. Quantifying Atmospheric Parameter Ranges for Ambient Secondary Organic Aerosol Formation. *ACS Earth Space Chem.* **2021**, *5* (9), 2380−2397.

(75) Isaacman-VanWertz, G.; Massoli, P.; O'Brien, R.; Lim, C.; Franklin, J. P.; Moss, J. A.; Hunter, J. F.; Nowak, J. B.; Canagaratna, M. R.; Misztal, P. K.; Arata, C.; Roscioli, J. R.; Herndon, S. T.; Onasch, T. B.; Lambe, A. T.; Jayne, J. T.; Su, L.; Knopf, D. A.; Goldstein, A. H.; Worsnop, D. R.; Kroll, J. H. Chemical Evolution of Atmospheric Organic Carbon over Multiple Generations of Oxidation. *Nat. Chem.* **2018**, *10* (4), 462−468.

(76) Kroll, J. H.; Lim, C. Y.; Kessler, S. H.; Wilson, K. R. Heterogeneous Oxidation of Atmospheric Organic Aerosol: Kinetics of Changes to the Amount and Oxidation State of Particle-Phase Organic Carbon. *J. Phys. Chem. A* **2015**, *119* (44), 10767−10783.

(77) O'Brien, R. E.; Kroll, J. H. Photolytic Aging of Secondary Organic Aerosol: Evidence for a Substantial Photo-Recalcitrant Fraction. *J. Phys. Chem. Lett.* **2019**, 7..

(78) Champion, W. M.; Rothfuss, N. E.; Petters, M. D.; Grieshop, A. P. Volatility and Viscosity Are Correlated in Terpene Secondary Organic Aerosol Formed in a Flow Reactor. *Environ. Sci. Technol. Lett.* **2019**, *6* (9), 513−519.

(79) Rothfuss, N. E.; Petters, M. D. Influence of Functional Groups on the Viscosity of Organic Aerosol. *Environ. Sci. Technol.* **2017**, *51* (1), 271−279.

https://doi.org/10.1021/acsestair.6c00059
ACS EST Air 2026, 3, 1421−1434